Supporting Information: Yeast Require Redox Switching in DNA Primase

O'Brien, E. †; Salay, L.E. †, et al.

Supplementary Materials and Methods

Figures S1 to S13

Tables S1 to S3

Supplementary Materials and Methods

Protein Expression and Purification. Yeast p58C (Pri2) residues 316-512 were cloned into pGB100 using the BamHI and NotI restriction sites. This plasmid was transformed into Rosetta DE3 cells. The cells were grown to an OD_{600} of 1.0 at 37 °C. They were then induced with 1 mM isopropyl β-D-1-thiogalactopyranoside (IPTG) and transferred to 20 °C for 16 hr. The cells were harvested and stored at -80 °C.

For purification, the cells pellets were thawed and resuspended in 50 mM NaH_2PO_4 (pH 7.8), 500 mM NaCl, 10 mM imidazole. Dnasin and lysozyme were added at 2 mg/g of cells. Protease inhibitor tablets (Roche) were added to the suspension. The suspension was homogenized using a Dounce homogenizer and then sonicated on ice for 10 min. The solution was spun at 50,000 rcf for 20 min at 4 °C. The supernatant was filtered and passed over a Ni- NTA column (GE Healthcare). The column was washed with 3 column volumes of 50 mM NaH_2PO_4 (pH 7.8), 500 mM NaCl, 20 mM imidazole. The protein was eluted with 50 mM NaH_2PO_4 (pH 7.8), 500 mM NaCl, 250 mM imidazole. The eluent was dialyzed overnight at 4 °C into 50 mM NaH_2PO_4 (pH 7.8), 500 mM NaCl, 10 mM imidazole and the 6xHis tag was cleaved using H3C protease. The dialyzed protein was repassed over the Ni-NTA column as in the previous step. The flow-through and wash fractions were collected. These fractions were dialyzed into 20 mM HEPES (pH 7.2), 50 mM NaCl, 2 mM dithiothreitol (DTT) (Heparin Buffer A), then was filtered and passed over a 5 ml Hi-Trap HP heparin column (GE Healthcare) that had been pre-equilibrated with Heparin Buffer A. The protein was eluted in Heparin Buffer B (20 mM HEPES (pH 7.2), 1 M NaCl, 2 mM DTT) using a linear gradient of 0 to 100% over 40 column volumes. The protein typically eluted at ~20% Heparin Buffer B (250 mM NaCl). The protein was dialyzed into 20 mM HEPES (pH 6.8), 2 mM DTT, and 200 mM NaCl, then flash frozen in N_2, and stored at -80 °C.

Site Directed Mutagenesis. Site directed mutagenesis for single-site and multi-site variants was performed using a Q5 mutagenesis kit (New England Biolabs). The primers to create the mutations are listed below. The same reverse primer was used for all mutations. The annealing temperature for amplification was 58 °C.

Site directed mutagenesis primers	
Mutation	Primer
Y395F	5’GAGAAGTTCAATAAAGAATTCCGTTACAGCTTCAGGC
Y397L	5’GAGAAGTTCAATAAAGAACTGCGTTACAGCTTCAGGC
Y397F	5’GAGAAGTTCAATAAAGAATACCGTTTCAGCTTCAGGC
Y397L	5’GAGAAGTTCAATAAAGAATACCGTCTGAGCTTCAGGC
Reverse primer	5’CATTGTCATGTTCCCATTTCTTGTAAATGC

Oligonucleotide preparation. All standard or modified phosphoramidites and DNA synthesis reagents were purchased from Glen Research. Unmodified DNA oligonucleotides for electrochemical experiments were purchased from Integrated DNA Technologies, Inc. DNA sequences for electrochemistry assays are shown in **Table S1**. Thiol-modified DNA strands for electrochemistry were made on an Applied Biosystems 3400 DNA synthesizer, with a C6 S-S phosphoramidite incorporated at the 5'- terminus. Single-stranded DNA was purified using standard procedures as described previously (1). High pressure liquid chromatography (HPLC) using a reverse-phase PLRP-S column (Agilent) was used, and oligonucleotide mass confirmed using MALDI-TOF Mass Spectrometry. Thiol-modified strands were reduced after the initial HPLC purification with 100 mM dithiothreitol (Sigma) for 2-3 h in 50 mM Tris-HCl, pH 8.4, 50 mM NaCl. Reduced thiol-modified DNA was purified by size exclusion chromatography (Nap5 Sephadex G-25, GE Healthcare) and subsequent reverse-phase HPLC. Single-stranded oligonucleotides were then desalted using ethanol precipitation and stored in low salt buffer (5 mM Phosphate, pH 7.0, 50 mM NaCl). Duplex DNA for electrochemistry was prepared by quantification of the complementary single-stranded oligonucleotides by UV-Visible spectroscopy, followed by annealing at 90 °C. A mixture of equimolar complementary single-stranded DNA (50 μM) was prepared in low salt buffer. Thiol-modified duplex DNA substrates were then deoxygenated by bubbling argon gas through the solution for 90-180 s. Duplex DNA was annealed on a thermocycler (Beckman Instruments) by initial heating to 90 °C, followed by slow cooling to 4 °C over 90 minutes. DNA was quantified using absorbance at 260 nm, with extinction coefficients at 260 nm for DNA obtained using Integrated DNA Technologies online OligoAnalyzer tool. Single-stranded DNA substrates were quantified using UV-Visible spectroscopy and stored in low salt buffer at a stock concentration for activity assays.

Multiplexed Chip Fabrication. DNA was prepared as described in the *SI Text.* Multiplexed electrode platforms were prepared using standard photolithography techniques, adapted from established protocols (1-3). Nine 1 in. by 1 in. chips were patterned on 525 um thick silicon wafers (SiliconQuest). A thermal oxide layer roughly 4000 Å thick was grown on the silicon wafers using a Tytan tube furnace (Tystar). S1813 photoresist (2 μm layer) was deposited onto the wafers for patterning of the chips before metal deposition. Electron beam evaporation (CHA Industries) was then used to deposit a 3 nm titanium adhesion layer followed by a 100nm gold layer, without breaking vacuum between depositions. Metal lift-off using Remover PG (MicroChem) was performed overnight (10-12 h) at room temperature. Wafers were subsequently dried with a nitrogen gun and dehydrated at 140 °C for 10 minutes. A 3 ∝m layer of insulating SU-8 photoresist was deposited and patterned onto the wafer as described previously (1-3), with connective wires between contact pads on the edges of the chips and working electrodes in the center were covered but the contact pads and working electrodes left exposed. This ensured a fixed working electrode surface area of 2 mM^2. SU-8 photoresist was cured (150 °C, 15 minutes) and wafers cleaved into individual chips using a Dynatex Scriber/Breaker or broken manually after scoring with a diamond tip scriber.

DNA-Modified Electrode Assembly/Preparation. Chips were dried thoroughly using argon gas and ozone-cleaned for 20 minutes at 20 mW using a Uvo brand ozone cleaner. Clean chips

were assembled onto polycarbonate holders with acrylic clamp and Buna-N rubber gasket according to previous protocols, with four quadrants in the chip separated by fastened gasket and clamp (1). Duplex DNA substrates, with a thiol modifier at the 5'- end, (25 µM) were deposited in a 20 µL volume onto each quadrant of the multiplex chip. Substrates incubated for 18-24 hours on the gold surface to allow formation of self-assembled DNA monolayer. DNA monolayers were washed with phosphate buffer (5 mM phosphate, pH 7.0, 50 mM NaCl, 5% glycerol) and subsequently backfilled with 1 mM 6-mercaptohexanol (Sigma) in phosphate buffer for 45 minutes. Monolayers are then washed 10 times per quadrant with phosphate buffer and twice per quadrant with TBP buffer (5 mM phosphate, pH 7.0, 50 mM NaCl, 4 mM $MgCl_2$, 4 mM spermidine) to aid in formation of a monolayer with termini accessible for p58C binding.

Sample preparation for electrochemistry. Wild type and mutant p58C samples were stored prior to experiments in p58C storage buffer (20 mM Tris, pH 7.2, 75 mM NaCl) or crystallography buffer (20 mM HEPES, pH 6.8, 200 mM NaCl, 2 mM DTT). All p58C variants were transferred to HEPES electrochemistry buffer (20 mM HEPES, pH 7.2, 75 mM NaCl) using Amicon ultra centrifugal filters (0.5 mL, 3MWCO) (Millipore Sigma). Protein was applied in a 90-140 µL volume to the filter and centrifuged for 15 minutes at 14000 x g at 4 °C. After centrifugation, 400 µL of HEPES electrochemistry buffer was applied to the filter and centrifuged at 14000 x g for 20 minutes. This was repeated four times to exchange the p58C protein into HEPES electrochemistry buffer. After buffer exchange and recovery of sample by centrifugation (2 minutes, 1000 x g), concentrations of [4Fe4S] cluster-containing p58C or mutants were measured using UV-Visible spectroscopy, by absorbance of the [4Fe4S] cluster at 410 nm (extinction coefficient = 17000 M^{-1} cm^{-1}) (4). Recovered samples (approx. 100-150 µL volume) were deoxygenated for 2-3 minutes with argon. Samples were then transferred into the anaerobic chamber (Coy Laboratory products). Before deposition onto the gold electrode surface, p58C/mutant samples were diluted to a molar concentration of 30 µM or 57 µM [4Fe4S] p58C variant with previously deoxygenated HEPES electrochemistry buffer.

Mutant Selection and Design. Mutations in the p58C domain of human DNA primase were designed based on previously determined structural data (5-8) bioinformatics (6) compiled for conserved residues in this domain. Chimera software was used to analyze the relevant residues in the 1.54 Å resolution structure of yeast p58C (6) (PDB 3LGB). Distances between tyrosine residues were measured between centroids.

Circular Dichroism. Near-UV circular dichroism was performed as described in (9).

Fluorescence anisotropy. Fluorescence anisotropy was performed as described in (3). Yeast p58C and the related mutants were assayed in a buffer containing 20 mM HEPES (pH 6.8), 2 mM DTT, and 75 mM NaCl.

DNA Electrochemistry Measurements of p58C Variants. Multiplex gold electrodes were part of a three-electrode system with an external Ag/AgCl reference electrode (Bioanalytical Systems) and platinum counter electrode. Initial cyclic voltammetry scans of the monolayers in p58C buffer were performed to ensure monolayer formation on each electrode. All washes were performed with 20 µL buffer volumes on each quadrant. Before scanning, a 200 µL volume was deposited over the chip surface, a bulk solution well for completion of a three-electrode circuit with an external reference and counter electrode. Cyclic voltammetry scans were performed at 100 mV/s scan rates, over a potential range of +0.412 V to -0.288 V vs. NHE or +512 mV to –188 mV vs NHE. Bulk electrolysis on DNA was performed at an applied potential of +0.412 V vs. NHE or +512mV vs. NHE for all electrochemical oxidation reactions and -0.188 V vs. NHE for all electrochemical reduction reactions. The oxidizing potential was applied for at least 8.33 minutes for single oxidation reactions on a surface, and 6.67 minutes for the iterative oxidation cycles of p58C variants. The reducing potential was applied for 8.33 minutes in all electrochemical reduction reactions. All bulk electrolysis and cyclic voltammetry was performed in previously deoxygenated p58C storage buffer (20 mM HEPES, pH 7.2, 75 mM NaCl). Charge transfer (nC) in the cathodic peak of oxidized samples CV scans was assessed using the area under the current wave of the reduction signal. Variants of p58C were compared for charge transfer proficiency using at least three trials of oxidation at +0.412 V vs. NHE or +512 mV vs. NHE, after at least 8.33 minutes of oxidation at the applied potential. Charge transfer was measured for oxidized samples using CHI software, assessing the area under the reductive peak in CV after electrochemical oxidation. Yields for bulk electrolysis were assessed by subtracting the total charge reported in Coulombs from the product of the electrolysis time (s) and the final current value (A). NTP-dependence of electrochemical signals were measured by pipetting a small volume (1-3 µL) of 0.1 M ATP stock solution into each quadrant of the multiplexed chip setup. These stocks should be added by quadrant, rather than into the bulk solution. Divide the NTP stock into quarters and pipet ¼ of the total solution onto a quadrant. Samples were added by quadrant, as physical barriers in the setup prevent diffusion of NTPs between electrode quadrants. After the volume of ATP stock was deposited onto the electrode quadrant, resulting in a 2.5 mM or 5 mM concentration of ATP in the quadrant, CV scans were measured at a 100 mV/s scan rate. Square wave voltammetry in both reductive and oxidative sweeps was measured using a symmetric square wave form (25 mV amplitude), superimposed on a staircase (E_{step} = 4 mV). Scans were performed at 15 Hz frequency, 60 mV/s scan rate. Charge transfer was assessed using CHI software; charge values were determined by calculation of the area under the reductive and oxidative peak curves. Midpoint potentials of NTP-dependent redox signals were assessed using the peak selection function in CHI software.

X-ray Crystallography. Crystals were grown at 16 °C by mixing 1:1 yeast p58C variants (~5 mg/ml) and mother liquor (100 mM TRIS (pH 8.5), 40-65% MPD) using hanging drop vapor diffusion. Crystals formed after 2 days. They were then looped, transferred to a cryo-protectant containing the mother liquor and 20% glycerol.

Data collection for yeast p58C Y397F was performed at 100 K using an in-house Bruker Microstar rotating anode x-ray generator with a Bruker Proteum PT135 CCD area detector at a wavelength of 1.54 Å. Sulfur single anomalous dispersion (SAD) was used to phase this data set with the program suite HKL2MAP (10). The model was built using arp/Warp in the CCP4 suite of programs (11) followed by iterative rounds of refinement using Phenix (12) and *Coot* (13)**.**

Crystallographic data for the remaining variants were collected at the Advanced Photon Source (Argonne National Laboratory, Chicago, IL) on Life Sciences Collaborative Access Team beamlines. Data were indexed and scaled using HKL2000 (14). Molecular replacement using Phaser (15) with the model of the yeast p58C variant Y397F was used to solve the phases of the remaining mutants. The models were refined iteratively using Phenix (12) and *Coot* (13). Access to these programs was provided by SBGrid (16).

Yeast Strain Construction. Integration plasmids were constructed by subcloning a *PRI2* C-terminal domain (CTD) fragment of plasmid PRI2-3HA (17,18) into the pRS406 vector (19) and mutations were created using overlap-extension PCR (20). Silent nucleotide changes were included to create restriction site polymorphisms tightly linked to each mutation. Plasmids linearized with *Age*I-HF (NEB) were transformed into YKF201 and Ura+ transformants were subsequently plated on media containing 5-fluoroorotic acid. Chromosomal integration of all mutations was verified by restriction digestion and sequencing (cells losing the *URA3* marker by recombination also lost the 3HA tag). To test for viability of the *pri2-Y395L* allele, strain YKF201 was transformed with the complementing plasmid pRS416-*PRI2,* containing a 3.1kb fragment amplified from yeast genomic DNA inserted at the *Bam*HI and *Eco*RI sites of pRS416. PRI2-3HA plasmids (either WT or containing the Y397F or Y497L alleles) were linearized with *Age*I-HF (NEB) and integrated at the *PRI2* locus with selection on media lacking uracil and tryptophan. Individual transformants were verified by PCR and sequencing, then restreaked on media lacking uracil and tryptophan to confirm growth and on media lacking tryptophan and containing 5-fluoroorotic acid (5-FOA) to select for loss of the complementing plasmid.

For inducible overexpression of PRI2 alleles, the open reading frame of *PRI2* was cloned into plasmid p416-Gal1 at the *Bam*HI and *Xba*I sites (21). The Y397L mutation was incorporated by subcloning from the integration plasmid described above. All plasmids were verified by sequencing. Overexpression plasmids were transformed into haploid strain YKF1675 (*MAT**a**::DEL.HOcs::HisG ura3 trp1 leu2::KAN hml::hisG HMRa-stk*; isogenic to strain CL11-7) (22) with selection on media lacking uracil. Individual transformants were restreaked on media lacking uracil and containing 2% glucose or galactose. Sequences of oligonucleotides utilized for cloning and mutagenesis are available by request.

References

1. Pheeney CG, Arnold AR, Grodick MA, Barton JK. (2013) Multiplexed Electrochemistry of DNA-Bound Metalloproteins. *J Am Chem Soc* 135(32); 11869-11878.

2. Slinker JD, Muren, NB, Renfrew SE, Barton JK. (2011) DNA charge transport over 34 nm. *Nat Chem* 3: 230-235.

3. O'Brien E, et al. (2017) The [4Fe4S] cluster of human DNA primase functions as a redox switch using DNA charge transport. *Science* 355(6327): eaag1789.

4. Cunningham RP, et al. (1989) Endonuclease III is an iron-sulfur protein. *Biochemistry* 28(10): 4450-4455.

5. Baranovskiy AG, et al. (2016) Mechanism of Concerted RNA-DNA Primer Synthesis by the Human Primosome. *J Biol Chem* 291(19): 10006-10020.

6. Sauguet L, Klinge S, Perera RL, Maman JD, Pellegrini L (2010) Shared active site architecture between the large subunit of eukaryotic primase and DNA photolyase. *PloS One* 5(4): e10083.

7. Vaithiyalingam S, Warren EM, Eichman BF, Chazin WJ (2010) Insights into eukaryotic priming from the structure and functional interactions of the 4Fe-4S cluster domain of human DNA primase. *Proc Natl Acad Sci USA* 107(31): 13684-13689.

8. Agarkar VB, Babayeva ND, Pavlov YI, Tahirov TH (2011) Crystal structure of the C-terminal domain of human DNA primase large subunit: implications for the mechanism of the primase-polymerase α switch. *Cell Cycle* 10(6):926-931.

9. Holt ME, Salay LE, Chazin WJ (2017) A Polymerase with Potential: The Fe-S Cluster in Human DNA Primase. *Methods in Enzymology* 595: 361-390.

10. Pape T, Schneider TR (2004) HKL2MAP: a graphical user interface for macromolecular phasing with SHELX programs. *J Appl Crystallogr* 37: 843-844.

11. Perrakis A, Sixma TK, Wilson KS, Lamzin VS (1997) wARP: Improvement and extension of crystallographic phases by weighted averaging of multiple-refined du mMy atomic models. *Acta Crystallogr D* 53 (4): 448-455.

12. Adams PD, et al. (2010) PHENIX: a comprehensive Python-based system for macromolecular structure solution. *Acta Crystallogr D Biol Crystallogr* 66: 213-221.

13. Emsley P, Lohkamp B, Scott WG, Cowtan K (2010) Features and development of Coot. *Acta Crystallogr D Biol Crystallogr* 66: 486-501.

14. Otwinowski Z, Minor W (1997) Processing of X-ray diffraction data collected in oscillation mode. *Methods Enzymol* 276: 307-326.

15. Mccoy AJ, et al. (2007) Phaser crystallographic software. *J Appl Crystallogr* 40: 658-674.

16. Morin A, Eisenbraun B, Key J, Sanschagrin PC, Timony MA, Ottaviano M, et al. Collaboration gets the most out of software. Elife. 2013;2:e01456.

17. Ricke RM, Bielinsky AK (2006) A conserved Hsp10-like domain in Mcm10 is required to stabilize the catalytic subunit of DNA polymerase-alpha in budding yeast. *J Biol Chem* 281(27): 18414-18425.

18. Liu L, Huang M (2015) Essential role of the iron-sulfur cluster binding domain of the primase regulatory subunit Pri2 in DNA replication initiation. *Protein Cell* 6(3): 194-210.

19. Sikorski RS, Hieter P (1989) A system of shuttle vectors and yeast host strains designed for efficient manipulation of DNA in *Saccharomyces cerevisiae*. *Genetics* 122(1): 19-27.

20. Warrens AN, Jones MD, Lechler RI (1997) Splicing by overlap extension by PCR using asymmetric amplification: an improved technique for the generation of hybrid proteins of immunological interest. *Gene* 186(1): 29-35.

21. Mumberg D, et al. (1994) Regulatable promoters of Saccharomyces cerevisiae: comparison of transcriptional activity and their use for heterologous expression. *Nucleic Acids Res* 22(25): 5767-5768.

22. Lydeard JR, Jain S, Yamaguchi M, Haber JE (2007) Break-induced replication and telomerase-independent telomere maintenance require Pol32. *Nature* 448(7155): 820–823.

23. Ji H, Platts MH, Dharamsi LM, & Friedman KL (2005) Regulation of telomere length by an N-terminal region of the yeast telomerase reverse transcriptase. Mol Cell Biol 25(20):9103-9114.

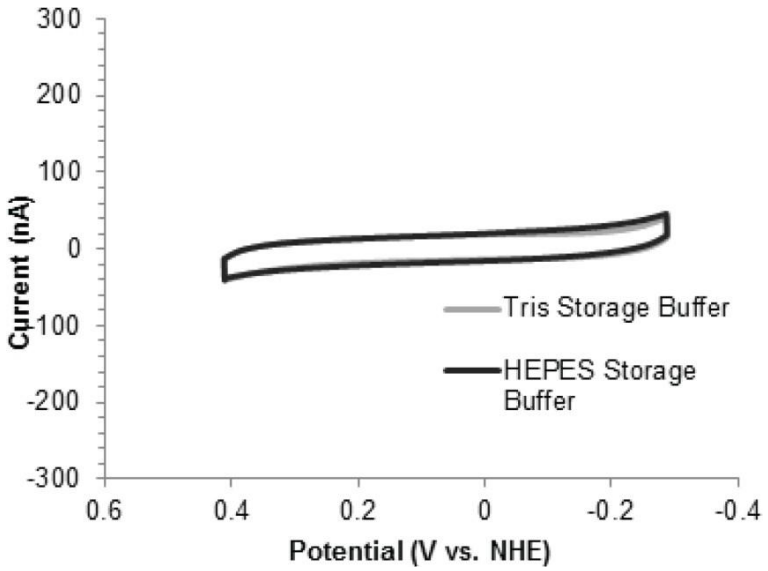

Figure S1. P58C does not produce a redox signal on ss/dsDNA in the absence of electrochemical alteration. CV performed on 30 µM [4Fe4S] p58C in Tris storage buffer (light grey trace) and 40 µM [4Fe4S] p58C in HEPES storage buffer (dark grey trace) using a Ag/AgCl reference electrode is shown. Buffer conditions were 20 mM Tris buffer, pH 7.2, 75 mM NaCl or 20 mM HEPES, pH 7.2, 75 mM NaCl. CV scanning was performed in anaerobic conditions, at a 100 mV/s scan rate, for both samples.

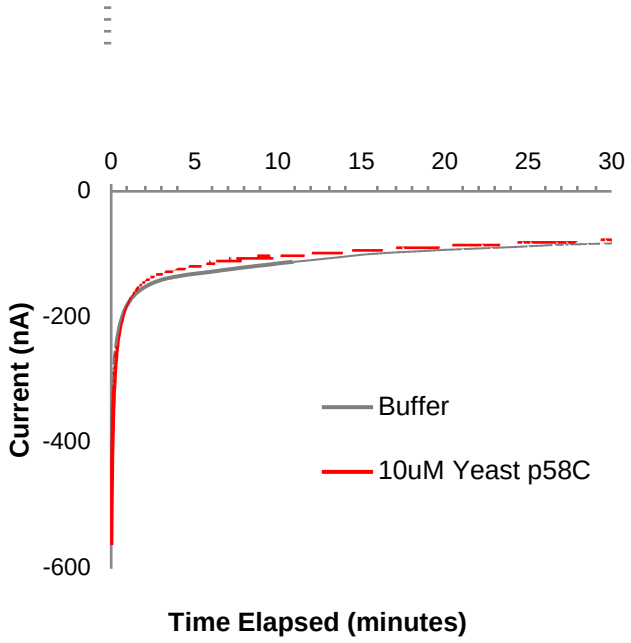

Figure S2. Bulk oxidation of WT p58C (*S. cerevisiae*), shown in red, compared to a buffer blank control (grey). The yield for oxidation is relatively low, but the technique is effective in converting the protein from the $[4Fe4S]^{2+}$ form to the $[4Fe4S]^{3+}$ form. Electrochemical oxidation was performed in anaerobic conditions at an applied potential of 512mV vs. NHE, on 10 mM [4Fe4S] p58C in 20 mM MES, pH 7.2, 75 mM NaCl, 10% glycerol.

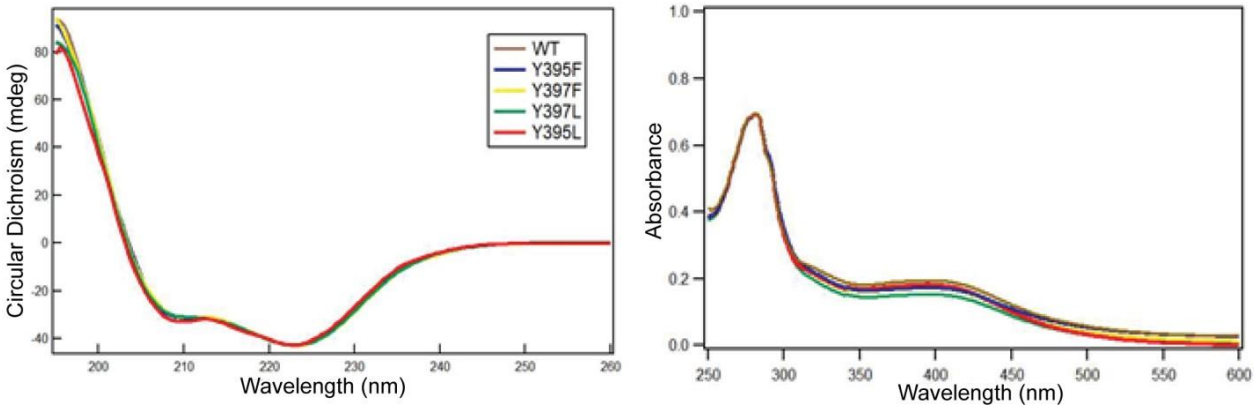

Figure S3. WT and mutant yeast p58C biophysical characterization. left) Circular dichroism (CD) spectroscopy of WT and mutant p58C indicate the mutations do not perturb any of the elements of secondary structure. All spectra normalized to WT at 222 nm. right) UV-Visible spectroscopy of WT and mutant p58C shows similar 280 nm/410 nm absorbance ratios, indicating similar degrees of [4Fe4S] cluster cofactor loading in all variants. All spectra normalized to WT at 410 nm.

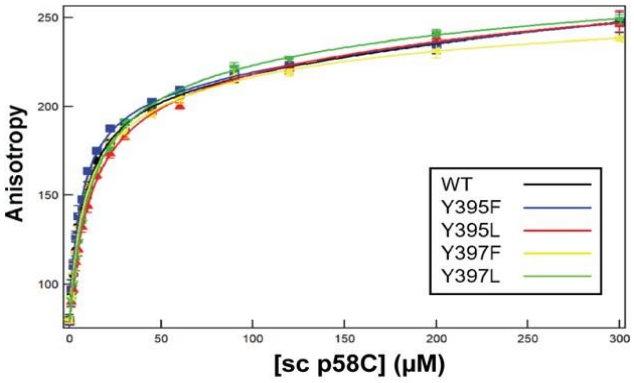

Dissociation Constants for Yeast p58C

Construct	K_d (μM)
WT	8.3±0.4
Y395F	6.1±0.6
Y395L	11.1±1.4
Y397F	7.2±1.0
Y397L	10.8±1.1

Figure S4. Fluorescence anisotropy measuring DNA binding of p58C variants. WT and tyrosine mutants bind DNA with similar affinity, suggesting that differences in electrochemical signals are due to differences in redox proficiency.

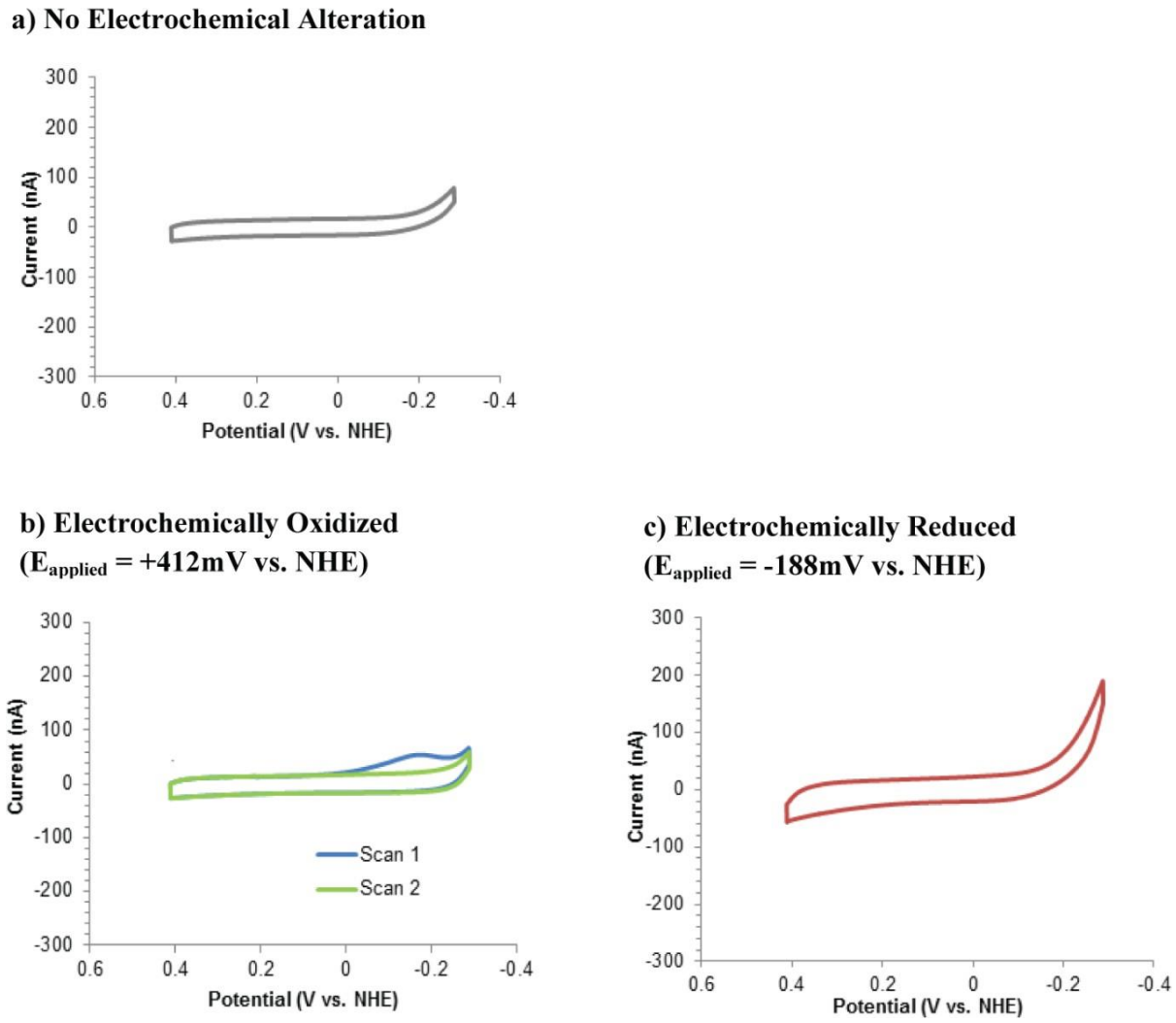

Figure S5. CV scans of yeast p58C Y395F. a) Electrochemically unaltered p58C Y395F mutant displays no electrochemical signal on DNA. b) p58C Y395F tyrosine mutant displays a cathodic peak after oxidation at an applied potential of +412 mV vs. NHE, but the peak is significantly smaller than that observed for wild type. c) p58C Y395F displays no redox signal on DNA after electrochemical reduction at an applied potential of -188 mV vs. NHE. All scans performed on 30 µM [4Fe4S] p58C Y395F, in 20 mM Tris, pH 7.2, 75 mM NaCl, at a 100mV/s scan rate.

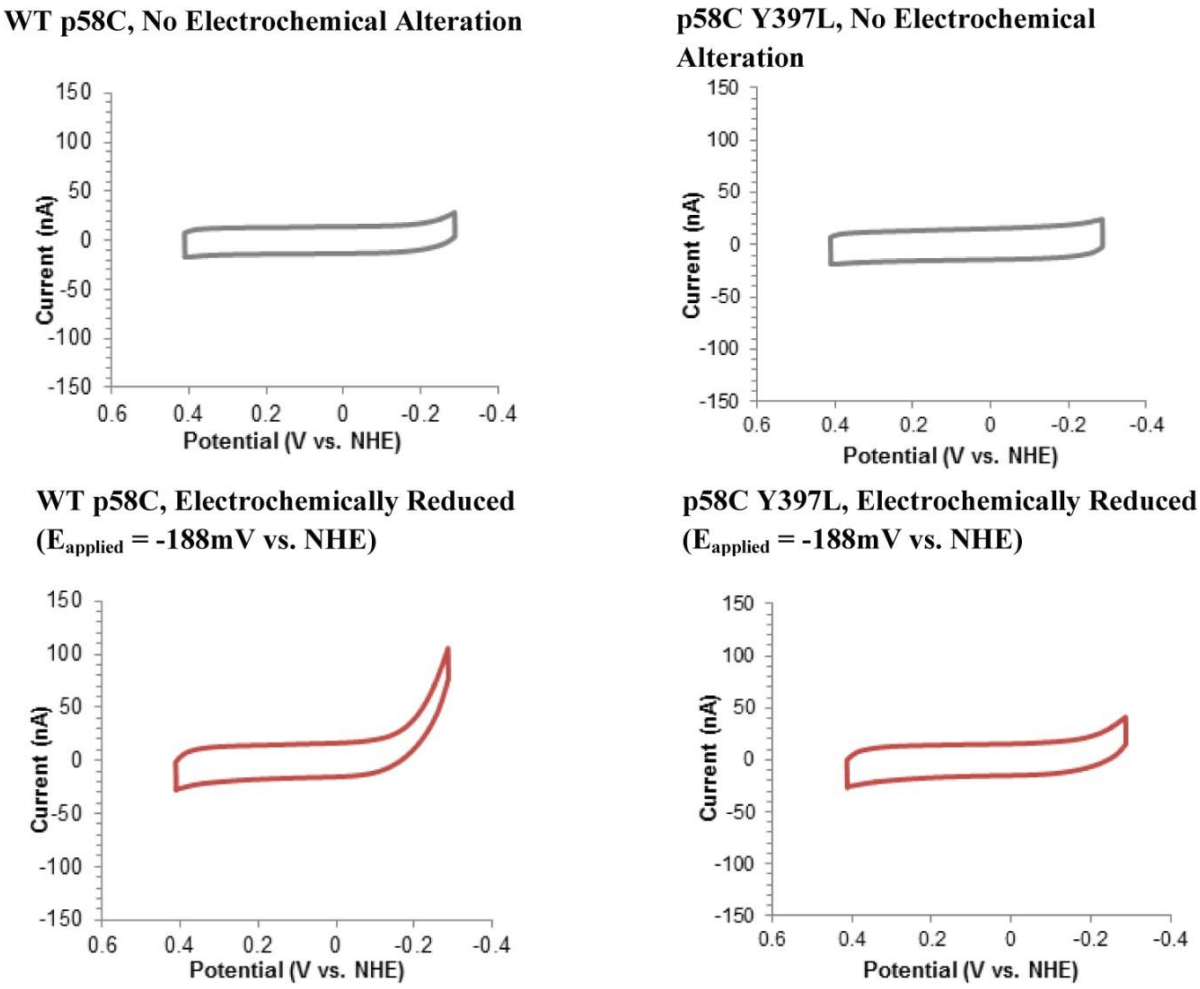

Figure S6. Cyclic voltammetry of electrochemically unaltered WT p58C (top left, grey trace) and p58C Y397L (top right, grey trace) and electrochemically reduced WT p58C (bottom left, red trace) and p58C Y397L (bottom right, red trace). Electrochemically unaltered and electrochemically reduced variants under identical conditions display no redox activity, suggesting that the unaltered samples is predominantly in the redox-inert, $[4Fe4S]^{2+}$ form. All CV scans were performed in anaerobic conditions, with 57 µM [4Fe4S] WT p58C or 40 µM [4Fe4S] Y397L in 20 mM HEPES, pH 7.2, 75 mM NaCl. Scans were performed at 100 mV/s scan rate.

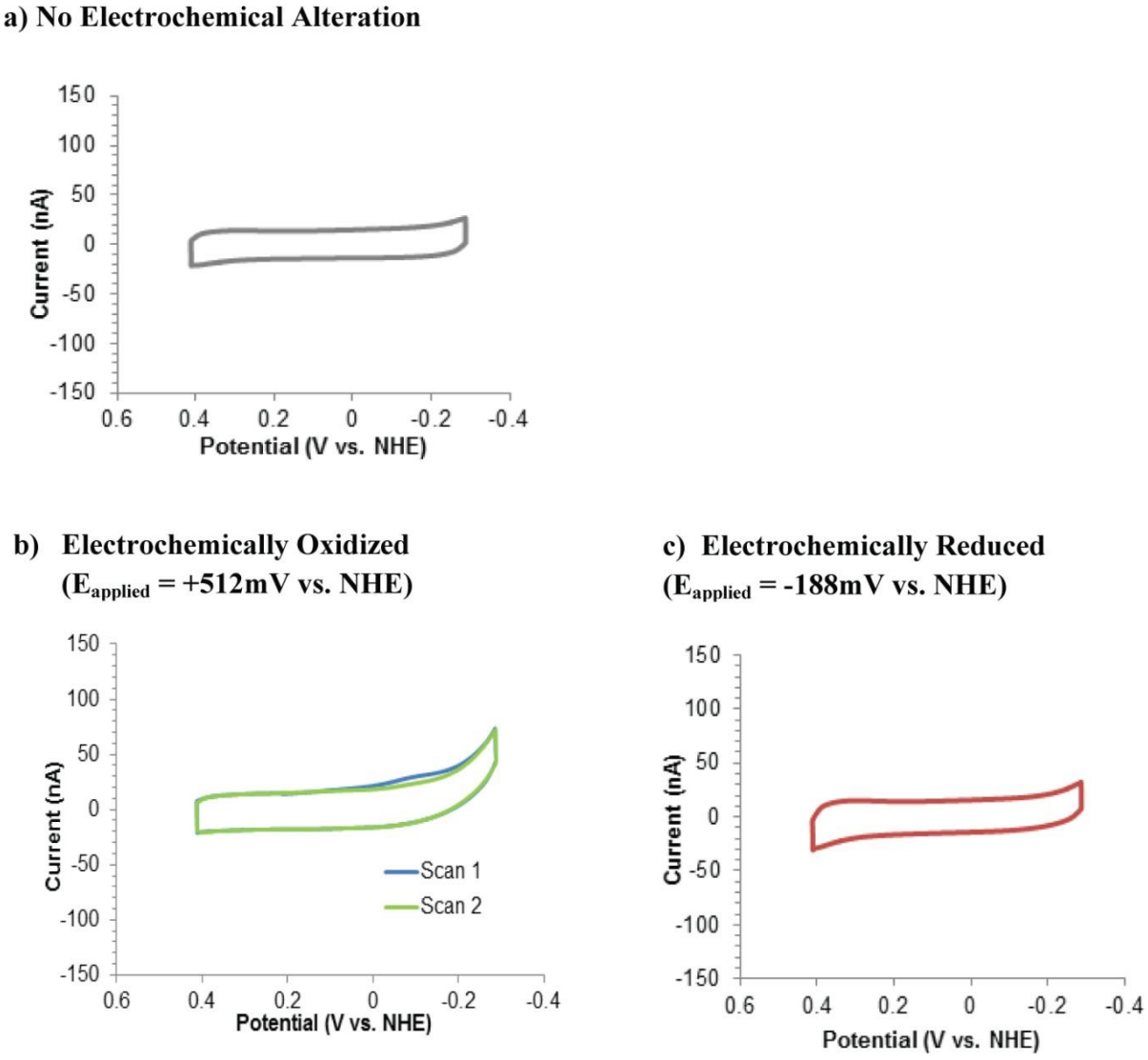

Figure S7. CV scans of yeast p58C Y395L. a) Electrochemically unaltered p58C Y395L mutant displays no electrochemical signal on DNA. b) p58C Y395L tyrosine mutant displays a cathodic peak after oxidation at an applied potential of +512 mV vs. NHE, but the peak is significantly smaller than that observed for wild type. c) p58C Y395L displays no redox signal on DNA after electrochemical reduction at an applied potential of -188 mV vs. NHE. All scans performed on 57 µM [4Fe4S] p58C variant, in 20 mM HEPES, pH 7.2, 75 mM NaCl, at a 100 mV/s scan rate.

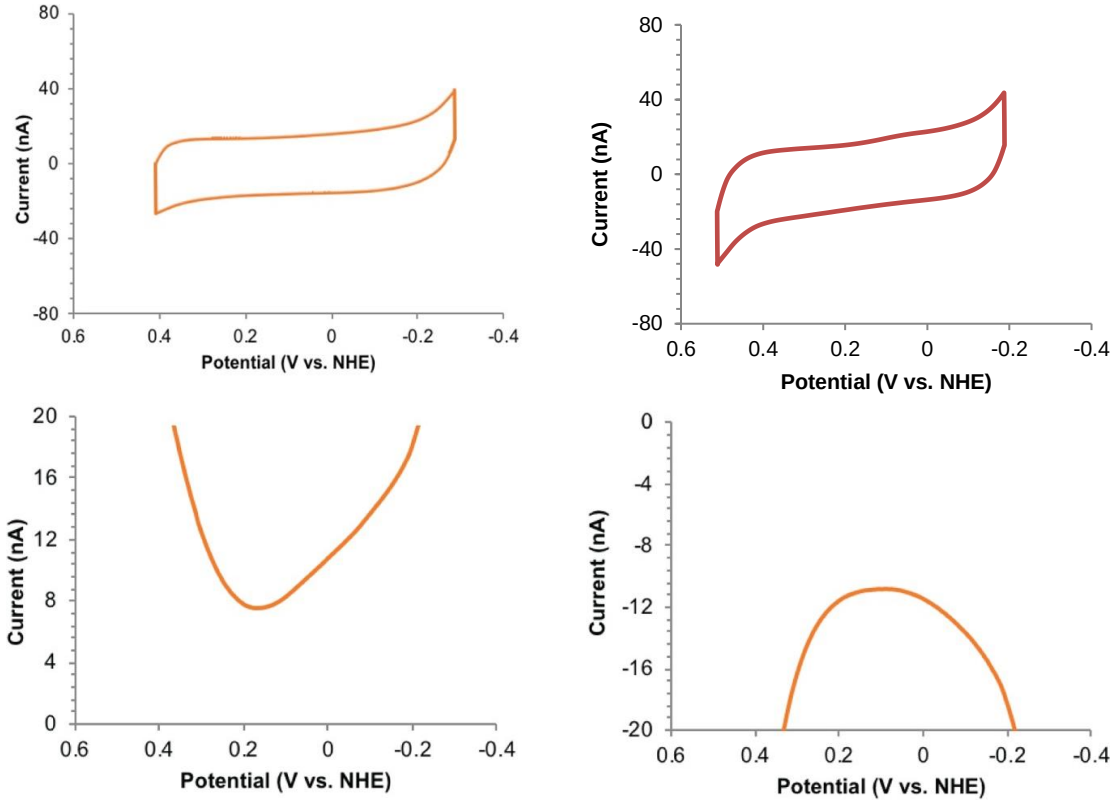

Figure S8. Electrochemistry of yeast p58C Y395L in the presence of 1.25 mM ATP (orange) and 2.5 mM ATP (red) CV scans (above) show no measurable redox signaling activity for p58C Y395L in the presence of DNA and NTPs. below) SWV of yeast p58C Y395L in the presence of 1.25 mM ATP. Reductive (left) and oxidative (right) scans show no measurable redox signaling activity in this variant. P58C Y395L is CT-deficient in the presence of DNA and NTPs. All scans performed in anaerobic conditions on 57 µM [4Fe4S] p58C Y395L and 1.25 mM ATP, in 20 mM HEPES, pH 7.2, 75 mM NaCl, at a 100 mV/s scan rate for CV or a 15 Hz frequency, 25 mV amplitude for SWV.

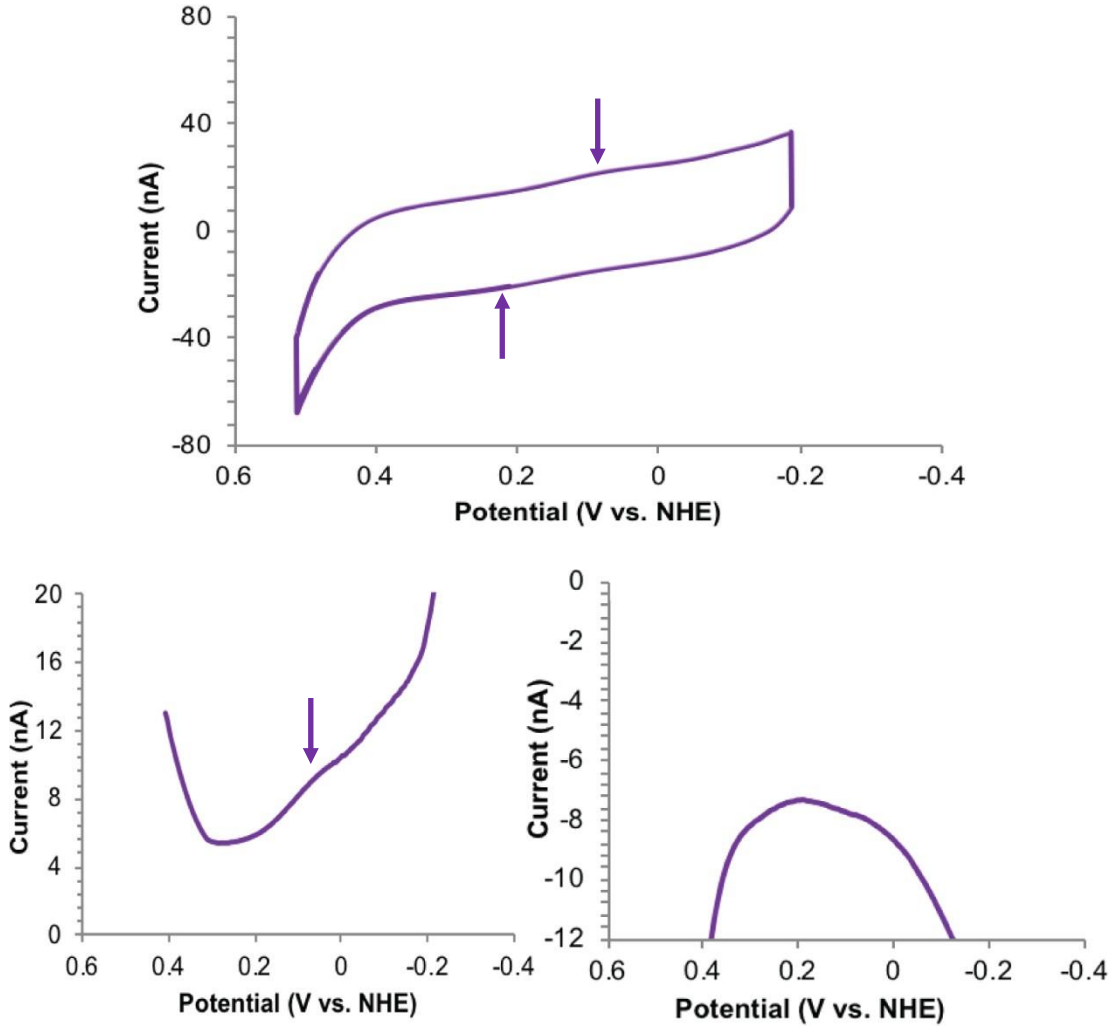

Figure S9. Electrochemistry of yeast p58C Y395F in the presence of 2.5 mM ATP. above) CV scans show some redox signaling activity in the presence of DNA and NTPs. Even in the presence of a higher concentration of ATP, this variant displays diminished redox signaling relative to WT. below) SWV of yeast p58C Y395F in the presence of 2.5 mM ATP. Reductive (left) and oxidative (right) scans show only a small amount of redox signaling activity in this variant. All scans performed in anaerobic conditions on 40 µM [4Fe4S] p58C Y395F and 2.5 mM ATP, in 20 mM HEPES, pH 7.2, 75 mM NaCl, at a 100 mV/s scan rate for CV or a 15 Hz frequency, 25 mV amplitude for SWV. Arrows indicate reductive and oxidative signals.

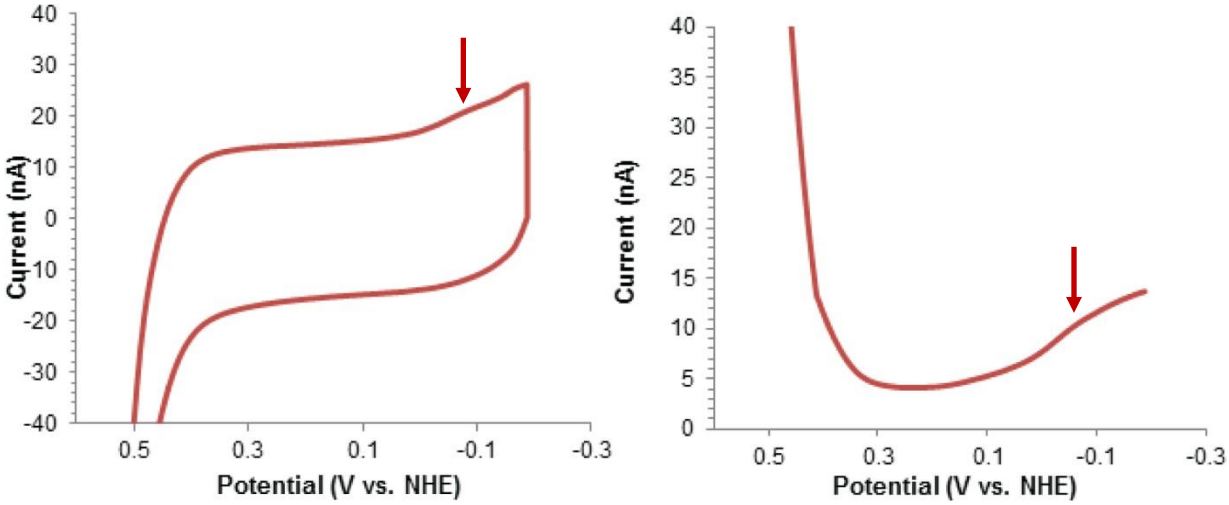

Figure S10. Electrochemistry of yeast p58C Y397F in the presence of 2.5 mM ATP. left) CV scans show a small peak in the reductive wave near -80 mV vs. NHE, which is likely a $[3Fe4S]^{+}$ oxidative degradation product. right) SWV of yeast p58C Y397F in the presence of 2.5 mM ATP. All scans performed in anaerobic conditions on 57 µM [4Fe4S] p58C Y397F and 2.5 mM ATP, in 20 mM HEPES, pH 7.2, 75 mM NaCl, at a 100 mV/s scan rate for CV or a 15 Hz frequency, 25 mV amplitude for SWV. Arrows indicate $[3Fe4S]^{+/0}$ reductive peak.

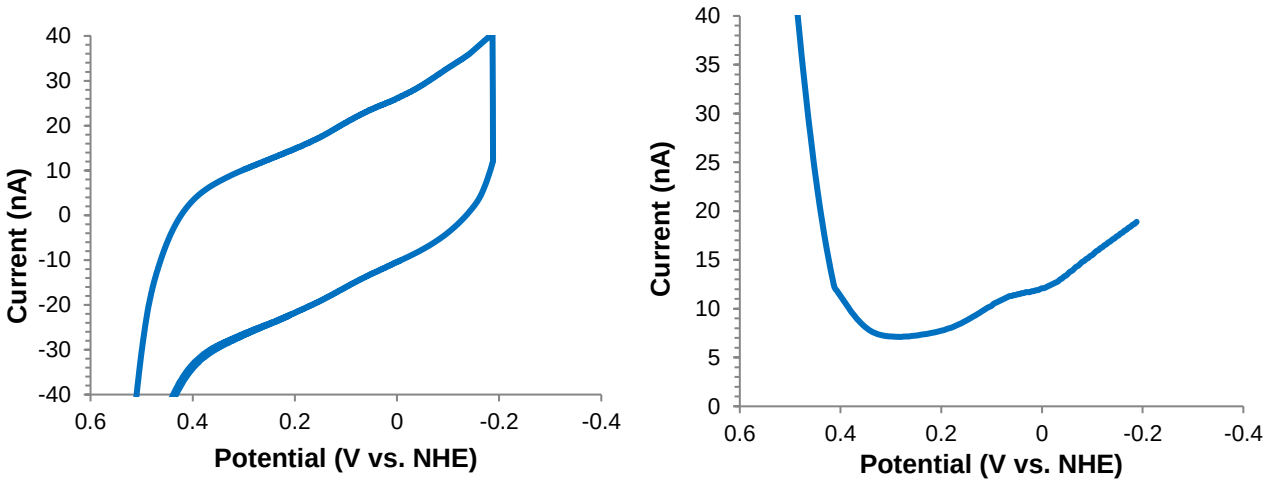

Figure S11. Electrochemistry of yeast p58C Y397L in the presence of 2.5 mM ATP. left) CV scans show a small reversible peak centered at 140 ± 17 mV vs. NHE. right) SWV of yeast p58C Y397L in the presence of 2.5 mM ATP. This variant shows a small amount of measurable redox signaling activity, though it is decreased from the redox signaling activity observed in WT yeast p58C. All scans performed in anaerobic conditions on 40 µM [4Fe4S] p58C Y397L and 2.5 mM ATP, in 20 mM HEPES, pH 7.2, 75 mM NaCl, at a 100 mV/s scan rate for CV or a 15 Hz frequency, 25 mV amplitude for SWV.

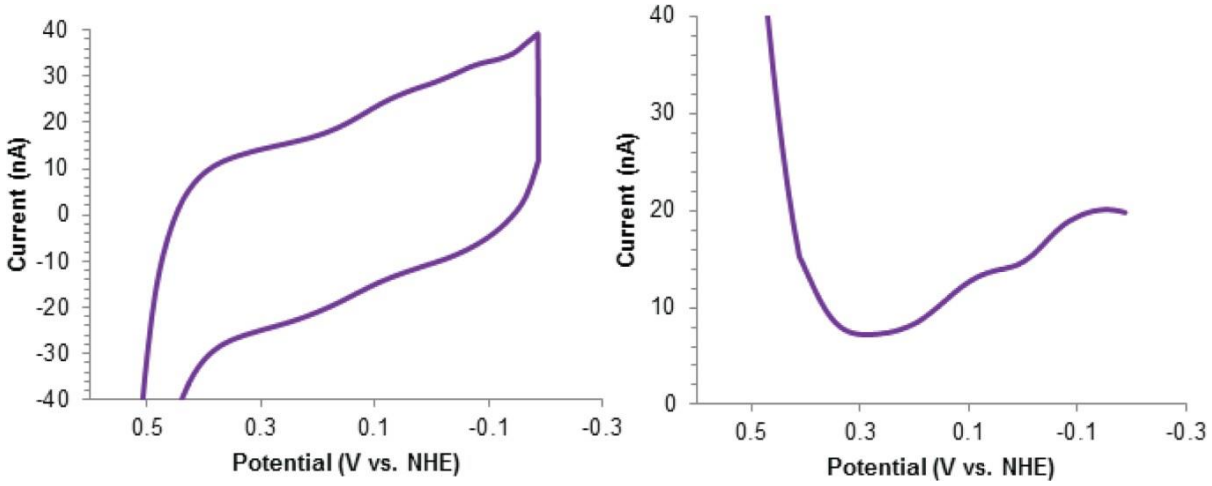

Figure S12. Electrochemistry of WT yeast p58C in the presence of 5 mM ATP. left) CV scans show a small peak in the reductive wave near -80 mV vs. NHE, likely a $[3Fe4S]^{+}$ oxidative degradation product. right) SWV of yeast p58C in the presence of 5 mM ATP. All scans performed in anaerobic conditions on 40 µM [4Fe4S] p58C and 5 mM ATP, in 20 mM HEPES, pH 7.2, 75 mM NaCl, at a 100 mV/s scan rate for CV or a 15 Hz frequency, 25 mV amplitude for SWV.

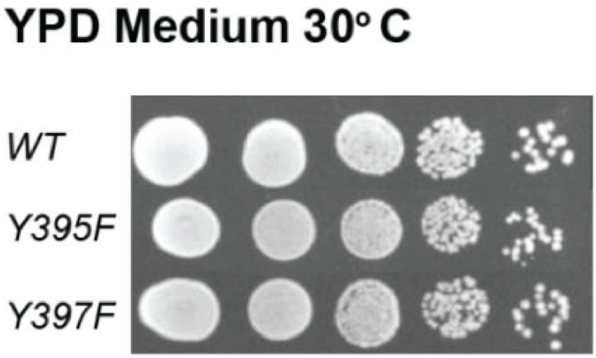

Figure S13. Yeast strains coding for WT *PRI2, pri2Y395F,* or *pri2Y397F*. Strains were grown in liquid rich medium overnight, normalized to OD_{600}= 1, and plated in ten-fold serial dilutions. Plated samples grew on agar plates for 2 days. All strains grew comparably in rich medium at permissive temperature (30 °C).

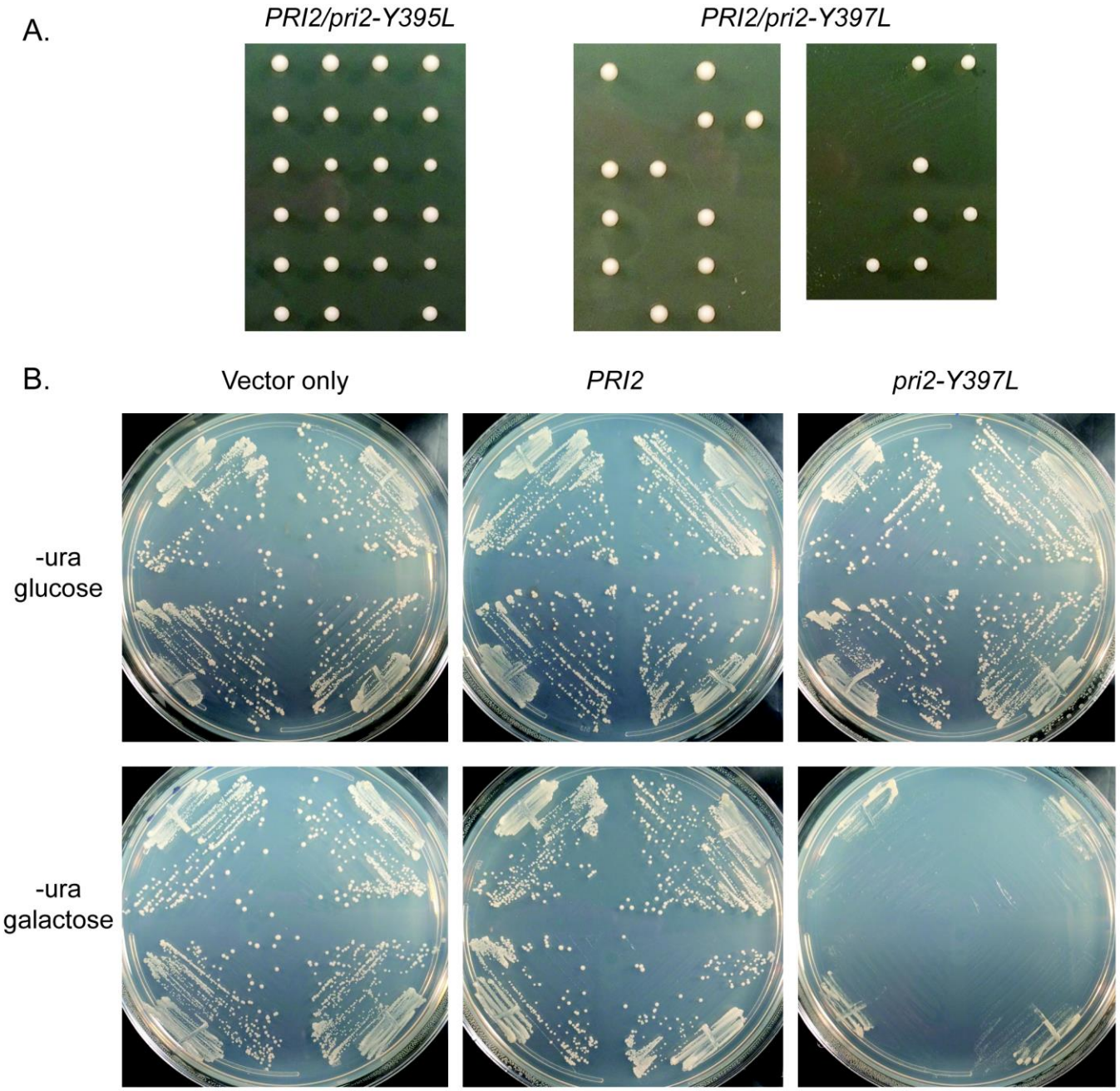

Figure S14. The non-viable *pri2-Y397L* allele causes synthetic lethality when over-expressed. (A) Mutation of Tyr397 (but not Tyr395) to leucine results in lethality. *Pri2* mutations were generated by two-step integration (Materials and Methods) in diploid strain DKF206 (*MATa/MATα trp1/trp1 leu2/leu2 ura3/ura3 his7/his7*). DKF206 is isogenic with YKF201 (23). Diploid strains heterozygous for *pri2-Y395L* or *pri2-Y397L* were verified by sequencing, sporulated, and tetrads were dissected by standard methods. All surviving segregants of the *pri2-Y397L* strain were confirmed to carry the wild-type *PRI2* allele. (B) Overexpression of *pri2-Y397L* inhibits cell growth. Empty vector (p416-Gal1) or p416-Gal1 containing wild-type *PRI2* or the *pri2-Y397L* allele were transformed into yeast and individual transformants were plated on media lacking uracil and containing glucose (top row, no induction) or galactose (bottom row, induction).

DNA Substrates	
p58C Electrochemistry	3'-CGCGTCTGTGCAACGTGCTG-SH-5' 5'-CATGCGCAGACACGTTGCACGAC-3'
p58C Fluorescence Anisotropy	3'-GAGAGTTT-5' 5'-[FitC]-TCTCTCTCTCAAA-3'

Table S1. Electrochemistry and fluorescence anisotropy DNA substrates used. Electrochemistry of p58C was performed on self-assembling monolayers of a 20-mer DNA duplex substrate with a 3-nt 5'- ssDNA overhang. Fluorescence anisotropy was performed on a 8-mer DNA duplex with a 5-nt ssDNA overhang. SH = $-(CH2)_6$-SH, FitC = FITC.

p58C Variant	Buffer	Concentration ([4Fe4S] protein)	E_{ox} (mV vs. NHE)	Q_{CV} (nC)
WT	Tris	30 µM	412	145±41
Y395F	Tris	30 µM	412	9.03±5.3
Y397F	Tris	30 µM	412	44.9±13
WT	HEPES	57 µM	512	2.19±0.33
Y395L	HEPES	57 µM	512	0.266±0.17
Y397L	HEPES	57 µM	512	0.732±0.15

Table S2. Summary of electrochemical oxidation conditions for yeast p58C variant assays on DNA-modified electrodes. Buffer conditions are 20 mM Tris, pH 7.2, 75 mM NaCl (Tris in table) or 20 mM HEPES, pH 7.2, 75 mMNaCl (HEPES in table). In HEPES buffer, protein samples were generally less redox-active than in Tris, which is likely due to some loss of [4Fe4S] cluster after buffer exchange. The charge transferred during CV (Q_{CV}) after bulk electrolysis is reported for each variant. WT moreover displayed greater Q_{CV} than variants tested at comparable conditions, suggesting that yeast p58C is less redox-proicient than human p58C but the redox activity depends on tunneling of charge through conserved tyrosines. Values reported are mean +/- S.D. for n=at least 3 trials.

Table S3: Crystallographic data collection and refinement statistics

	WT	Y395F	Y395L	Y397F	Y397L
Data Collection					
Wavelength	1.07807	0.98782	0.97856	1.54184	1.078
Space group	P 21 21 21	P 21 21 21	P 21 21 21	P 21 21 21	P 21 21 21
Resolution range	30.32 - 1.39 (1.44 - 1.39)	24.48 - 1.12 (1.16 - 1.12)	29.26 - 1.82 (1.88 - 1.82)	22.12 - 1.36 (1.41 - 1.36)	31.90 - 1.32 (1.37 - 1.32)
Cell dimensions					
a, b, c (Å)	41.09, 50.77, 89.83	40.99, 50.87, 89.91,	38.46, 50.83, 90.18	40.81, 50.81, 90.04	40.95, 50.87, 89.62
α, β, γ (°)	90, 90, 90	90, 90, 90	90, 90, 90	90, 90, 90	90, 90, 90
Reflections					
Total	73655 (6688)	143868 (12902)	31456 (2754)	77970 (7012)	88564 (8503)
Unique	37491 (3464)	72515 (6689)	16031 (1494)	40483 (3945)	44430 (4291)
Completeness (%)	96.80 (91.44)	98.52 (91.89)	96.80 (92.26)	98.68 (97.87)	99.53 (98.19)
R_{merge}	0.0313 (0.1033)	0.0253 (0.2132)	0.0253 (0.1956)	0.0458 (0.3282)	0.0275 (0.0822)
R_{meas}	0.0442 (0.146)	0.0358 (0.302)	0.0357 (0.277)	0.0648 (0.464)	0.0389 (0.116)
$CC_{1/2}$	0.997 (0.968)	0.999 (0.911)	0.997 (0.946)	0.998 (0.796)	0.997 (0.981)
Multiplicity	2.0 (1.9)	2.0 (1.9)	2.0 (1.8)	1.9 (1.8)	2.0 (2.0)
Mean I/σ (I)	11.59 (5.34)	12.18 (3.15)	7.54 (3.64)	12.72 (2.21)	19.43 (6.73)
Refinement					
No. of non-H atoms	1816	1794	1465	1756	1800
Macromolecules	1609	1590	1431	1563	1574
Ligands	24	24	32	32	24
Solvent	183	180	2	161	202
R_{work}/R_{free}	0.125/0.146 (0.109/0.158)	0.128/0.139 (0.197/0.194)	0.272/0.318 (0.424/0.427)	0.156/0.178 (0.232/0.257)	0.122/0.144 (0.119/0.150)
RMSD (bonds, Å)	0.011	0.018	0.018	0.012	0.014
RMSD (angles, °)	1.32	1.71	1.08	1.45	1.49
Ramachandran					
Favored (%)	98.88	98.89	96.55	98.33	97.77
Allowed (%)	1.12	1.11	3.45	1.67	2.23
Outliers (%)	0	0	0	0	0
Rotamer outliers (%)	0.57	0.57	0	0.59	0.57
Clashscore	1.53	3.1	5.25	0.95	5.01
Wilson B-factor ($Å^2$)	10.75	12.1	30.16	9.31	11.26
Average B-factor (Å)	16.04	18.91	60.07	15.1	17.6
Macromolecules	14.24	17.59	60.09	13.9	15.96
Ligands	25.41	22.22	58.66	24.55	23.14
Solvent	30.63	30.13	68.61	24.84	29.66
PDB Accession Code	6DI6	6DTV	6DU0	6DTZ	6DI2

Table S3. Crystallographic data for *S. cerevisiae* WT p58C (PDB 6DI6), p58C Y395F (PDB 6DTV), p58C Y395L (PDB 6DU0), p58C Y397F (PDB 6DTZ), and p58C Y397L (PDB 6DI2).